Appl. Phys. A (2017) 123:427
DOI 10.1007/s00339-017-1043-x

Applied Physics A
Materials Science & Processing

Novel phenomenon of magnetism and superconductivity in Fe-doped superconductor $Bi_{4-x}Fe_xO_4S_3$ ($0 \leq x \leq 0.1$)

Qing Li[1,2] · Difei Wang[1] · Zhenjie Feng[1,2,3] · Chuan Yu[1] · Hao Chu[4] · Xunqing Yin[1] · Jian Kang[1] · Cheng Cheng[1] · Xiaolong Li[5] · Dongmei Deng[1] · Chao Jing[1] · Shixun Cao[1,2,3] · Jincang Zhang[1,2,3]

Received: 11 March 2017 / Accepted: 14 May 2017 / Published online: 19 May 2017

Abstract We report the effects of Fe doping on the BiS_2-based superconductor $Bi_4O_4S_3$. It has been found that the superconducting transition temperature (T_C^{onset}) is slightly enhanced by Fe doping. The magnetic susceptibility results reveal the coexistence of superconductivity and long-range ferrimagnetism in these samples. A new magnetic transition temperature T_V (Verwey transition) from the *M*–*T* curves at ~112 K is observed. The isothermal magnetization curves (*M*–*H*) indicate a weak ferrimagnetism, which is probably due to the antiparallel ordering of Fe^{2+} and Fe^{3+} magnetic moments. The coexistence of superconductivity and ferro/ferrimagnetism makes bismuth oxysulfide superconductor a platform for understanding superconductivity from a new perspective.

✉ Zhenjie Feng
fengzhenjie@shu.edu.cn

✉ Xiaolong Li
lixiaolong@sinap.ac.cn

1 Department of Physics, Shanghai University, Shanghai 200444, China

2 Materials Genome Institute, Shanghai University, Shanghai 200444, China

3 Shanghai Key Laboratory of High Temperature Superconductors, Shanghai 200444, China

4 Department of Applied Physics, California Institute of Technology, Pasadena, CA 91125, USA

5 Shanghai Institute of Applied Physics, Chinese Academy of Sciences, Shanghai 201204, China

1 Introduction

The discovery of cuprates and iron based superconductor has aroused wide interest in search for new superconductors and provides us with a new research field on physics [1–3]. Recently, Mizuguchi et al. [4] report a new superconductor with $T_C = 4.5$ K in bismuth oxysulfide, $Bi_4O_4S_3$. $Bi_4O_4S_3$ is composed of stacking of a $Bi_4O_4(SO_4)_{0.5}$ spacer layer and two BiS_2 layers. There are 50% defects on SO_4 sites in $Bi_4O_4S_3$, while the inception compound $Bi_6O_8S_5$ free of SO_4 defects is an insulator. Band structure calculation shows the Fermi level mainly originates from the BiS_2 layer [4]. $Bi_4O_4S_3$ is a mixture of two structural phases, the superconducting $Bi_3O_2S_3$ phase with $T_C = 4.5$ K and the non-superconducting Bi_2OS_2 phase which acts as blocking layer in the superconducting $Bi_3O_2S_3$ phase. Morice et al. [5] studied the effect of blocking layers. The experimental results indicate a bulk superconducting behavior in this compound [6, 7]. And then several new BiS_2-based superconductors $(La/Nd/Ce/Pr)O_{1-x}F_xBiS_2$ [8–13] and $Sr_{1-x}La_xFBiS_2$ [14, 15] with the highest T_C of 11 K have been reported and studied. In addition, the Bi-oxide superconductor $Ba_{1-x}K_xBiO_3$ has a T_C of ~30 K [16]. As we know, the large Bi–Bi bonding plays an important role in superconductivity. Based on similarities of crystal structures and compositions to the layered high-T_C superconductors, it is proposed that T_C can be increased by optimizing the superconducting layers or structure of blocking in this family.

Furthermore, the relationship between magnetism and superconductivity is an important issue in strongly correlated electron systems. In copper oxides, carrier doping into Mott insulators suppresses the magnetic order and induces high temperature superconductivity [17]. In iron based superconductor, superconductivity also emerges

after the magnetic state is destroyed. For example, in LaFeAsO, the partial substitution of F in O sites suppresses the antiferromagnetic order and induces higher transition temperature T_C. In some compounds, magnetism can coexist microscopically with superconductivity [18]. Extensive studies have shown that the quantum spin fluctuations associated with the magnetic order are important for superconductivity [19, 20].

Recently, some groups have observed the coexistence of ferromagnetism and superconductivity in $Sr_{0.5}Ce_{0.5}FBiS_2$ and $CeO_{1-x}F_xBiS_2$ at low temperature [21, 22]. In our previous works of Mn, Co, Ni-doped $Bi_4O_4S_3$ superconductors [23–25], the results reveal the coexistence of ferromagnetism and superconductivity. In this paper, the effect of replacing Bi with magnetic Fe ion on superconductivity in polycrystalline samples $Bi_{4-x}Fe_xO_4S_3$ ($0 \le x \le 0.1$) has been reported. The structural, magnetic and electronic transport properties were measured on as prepared samples. The coexistence of long-range ferrimagnetism and superconductivity in $Bi_{4-x}Fe_xO_4S_3$ ($0 \le x \le 0.1$) system is observed for the first time.

2 Experimental procedure

The bulk polycrystalline $Bi_{4-x}Fe_xO_4S_3$ ($0 \le x \le 0.1$) samples are prepared using solid-state reaction technique. Firstly, the stoichiometric amounts of Bi_2S_3 (99.99%), Bi_2O_3 (99.99%), S (99.999%), and Fe_2O_3 (99.9%) were weighed and ground in a glove box under argon atmosphere. Then we press and seal the mixture in an evacuated quartz tube. Afterwards, the quartz tube is heated at 510 °C for 10 h. The second step is repeated to ensure good homogeneity. Then the pellets are cooled to room temperature.

The crystal structures are characterized by X-ray powder diffraction (XRD, 18 kW D/MAX 2550) using the Cu-$K\alpha$ radiation at room temperature. Resistance is measured by four-point probe method. The magnetization measurements are performed on the physical property measurement system (PPMS, Quantum Design). Magnetization temperature (M–T) curves are measured from 3 to 300 K in the zero-field-cooled (ZFC) mode and the field-cooled (FC) mode with an applied magnetic field of 100 Oe.

3 Results and Discussion

Figure 1a shows the X-ray diffraction patterns of the $Bi_{4-x}Fe_xO_4S_3$ ($0 \le x \le 0.1$) samples. The diffraction peaks were indexed with the tetragonal structure (space group: I4/mmm). From the XRD results, it is found that all the Fe-doped samples have similar pattern to the pristine

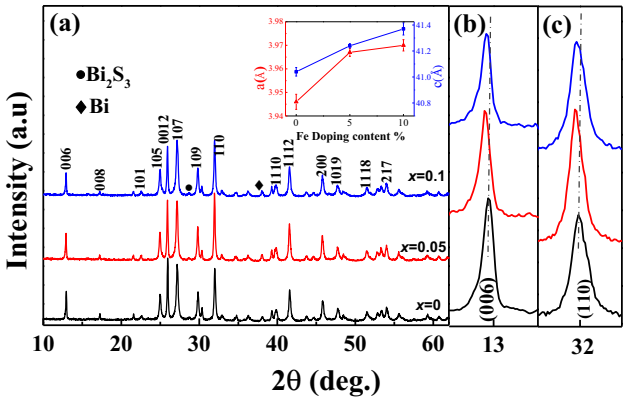

Fig. 1 **a** Room temperature, power X-ray diffraction patterns for $Bi_{4-x}Fe_xO_4S_3$ ($0 \le x \le 0.1$), Miller indices are displayed for the $Bi_{3.9}Fe_{0.1}O_4S_3$ sample. The *inset* shows the doping dependent variations of the in-plane and c-axis lattice parameters **a** and **c**. **b** The enlarged details around the (006) peak for all samples. **c** The enlarged details around the (110) peak for all samples

$Bi_4O_4S_3$ with a few peaks of the impurity phase. For further investigations, we represent the variation of the lattice parameters with the Fe doping level (x) in the inset of Fig. 1a. The enlarged view of (110) and (006) peaks are also given in Fig. 1b, c, respectively. We can see that, both the (110) and (006) peaks shift towards lower angles when $x = 0.05$ and 0.1. It indicates the successful substitution of Fe ion doping and an increase in the lattice constants is shown on the inset of Fig. 1a. We have also prepared and characterized higher Fe-doped ($x = 0.15$) sample, those two peaks were not shifted towards lower angles and the abnormal peaks may be caused by the out of range doping level in these samples. A minority of Bi_2S_3 and Bi impurities appears in all samples, which is common in solid-state reaction method of title compound [4, 7].

Figure 2a shows the DC magnetization of the $Bi_{4-x}Fe_xO_4S_3$ ($0 \le x \le 0.1$) samples under zero-field-cool (ZFC) from 3 to 300 K with an applied field $H = 100$ Oe. With the temperature decreasing, an anomaly is observed in DC magnetization around 112 K on FC curves and the ZFC and FC curves diverges in all doping samples. For each magnetization curve, two temperature points are noteworthy: the first one is the Verwey temperature (T_V) near $\sim$112 K for all samples except $x = 0$, where a local dM/dT maximum occurs as shown in Fig. 2c, noted as the transition between weak ferromagnetism and ferrimagnetism. This type of Verwey temperature can also be seen as the shift of the transition temperature in magnetite nanoparticles [26]. The Verwey temperature (T_V) in the ZFC curves starts to appear first and then decreases with increasing doping concentration x as shown in Fig. 2c. The other noteworthy temperature is the superconducting transition temperature (T_C) which is observed from the rapid drop in the magnetization. Figure 2b is the zoom-in of the

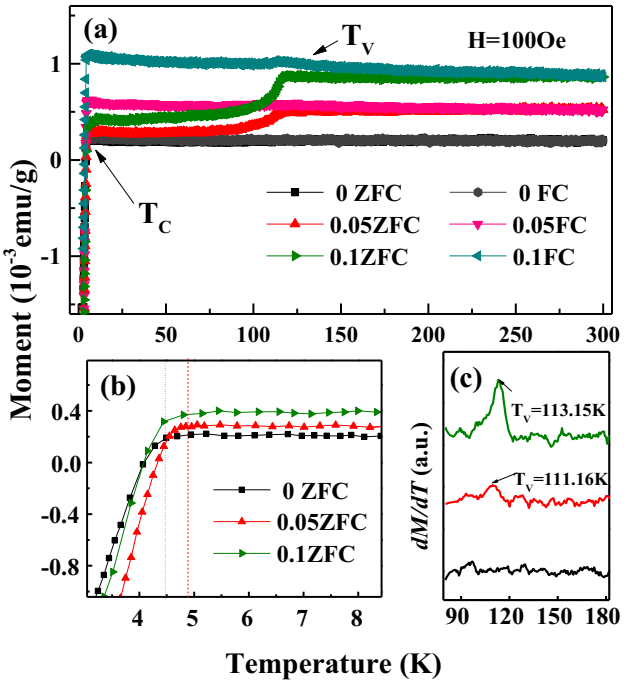

Fig. 2 Temperature dependent magnetization of $Bi_{4-x}Fe_xO_4S_3$ ($0 \le x \le 0.1$) samples. **a** Zero-field-cool (ZFC) and field-cool (FC) magnetization as a function of temperature is shown in the main panel from 3–300 K with an applied field $H = 100$ Oe. **b** The enlarged view of the temperature dependence of ZFC-magnetization for all samples at $H = 100$ Oe in the lower-temperature region. **c** Temperature dependent dM/dT for all samples for the temperature range of 80–180 K, showing single-peak feature for all samples except $x = 0$

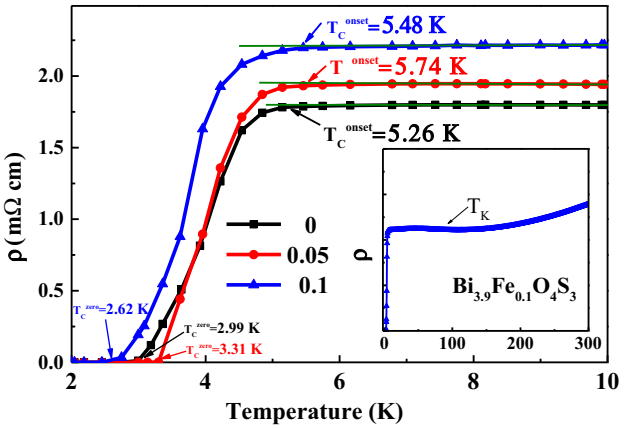

Fig. 3 Temperature dependence of the resistivity under zero magnetic field. $Bi_{4-x}Fe_xO_4S_3$ ($0 \le x \le 0.1$) samples in the temperature range of 2–10 K. The inset shows the full temperature range of 2–300 K for $Bi_{3.9}Fe_{0.1}O_4S_3$ sample

temperature dependence of magnetization in the ZFC curves for all samples in the lower-temperature region. Superconducting signal appears at 4.5 K in the $Bi_4O_4S_3$ sample. With increasing doping concentration, T_C gradually increases to the maximum at $T_C = 4.87$ K in $Bi_{3.95}Fe_{0.05}O_4S_3$ sample, and then gradually decreases to $T_C = 4.72$ K in $Bi_{3.9}Fe_{0.1}O_4S_3$. These facts suggest that slight Fe doping enhances the superconductivity of $Bi_4O_4S_3$ especially when $x = 0.05$, and then suppresses superconductivity. Those results also reveal that ferrimagnetism order can coexist with superconductivity in the $Bi_{4-x}Fe_xO_4S_3$ ($0 \le x \le 0.1$) system.

To improve the understanding for interplay of magnetism and superconductivity in $Bi_{4-x}Fe_xO_4S_3$ ceramics, we measure resistivity (ρ) vs Temperature. The temperature dependence of the resistivity for $Bi_{4-x}Fe_xO_4S_3$ samples were measured by four-point method under zero magnetic fields. Figure 3 shows the enlarged view of ρ–T curve below 15 K, the superconducting transition temperature T_C^{onset} and T_C^{zero} are defined as the onset and finish of the drop in the resistivity. The superconducting transition temperature shifts to slightly higher temperature with increasing the doping concentration of x, and reach its maximum when $x = 0.05$, then it shifts to lower temperatures with further x. This result is consistent with the DC magnetization measurement. Additionally, it is found that the normal-state resistivity of Fe ion doped samples increase with increasing doping concentration as shown in the inset of Fig. 3, suggesting a metallic behavior at high temperature. It resembles well with our previous studies which is related to under doped Mn ion substitution [25], Fe-doped samples can also exhibit a resistive upturn [27] at $\sim$90 K. A possible mechanism for the resistive upturn may be due to the occurrence of Kondo resonance at $T < T_K$, where T_K notes the Kondo temperature. In Mn-doped samples [25], we deliberate that a lower T_K with higher Mn-doping level would form due to stronger ferromagnetism. Our present study regarding Fe-doped samples agrees well with this interpretation, for Fe ion substitution introduced a long-range ferrimagnetism with smaller magnetic moment which is due to the different magnetic moment of Fe^{2+} and Fe^{3+} ions.

We have summarized that the Fe substitution dependence of ferrimagnetism and superconductivity in a comparison for $Bi_{4-x}Fe_xO_4S_3$ samples in Fig. 4a. T_C (M), determined from the onset of drop of ZFC-magnetization, is consistent with the T_C^{onset} (ρ) from resistivity data. T_C (ρ), T_C (M) and T_V all increases gradually to maximum when $x = 0.05$ and $x = 0.1$, and decreases with further substitution of x. The long-range ferrimagnetism in the Fe-doped samples may be interpreted as the *RKKY* interaction [28]. Figure 4b shows the comparison of the T_C (ρ), T_C (M), T_V and T_{Curie} for different 3d transition-metal ions substitutions in $Bi_4O_4S_3$ ceramic. The values of T_C (ρ) and T_C (M) exhibit little changes from those of $Bi_4O_4S_3$ compound. On the other hand, the different positive saturation magnetizations (T_{Curie}) and Verwey temperatures through different magnetic ions could give rise to magnetism orders

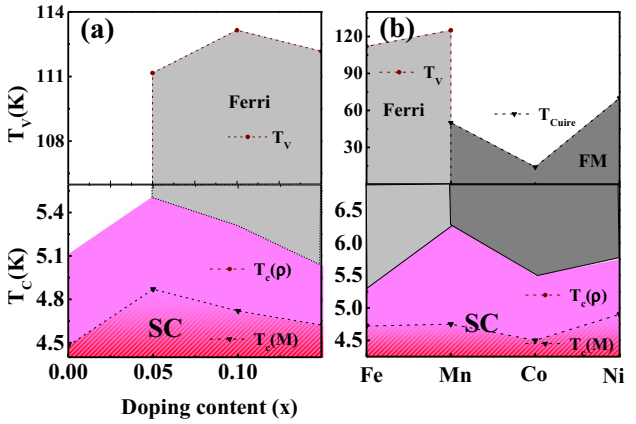

Fig. 4 Comparison of resistive and magnetic characterizations of $Bi_{4-x}A_xO_4S_3$ (A = Co, Ni, Mn and Fe, $x = 0.1$): **a** the nominal Fe concentration x via Verwey temperature and superconducting comparison for $Bi_{4-x}Fe_xO_4S_3$ ($0 \le x \le 0.1$) samples, respectively. **b** Comparison of the $T_c(M)$, $T_c(\rho)$, T_V and T_{Curie} for different 3d transition-metal substitutions

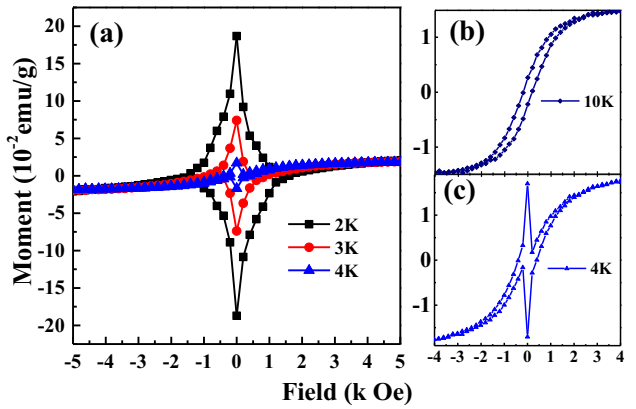

Fig. 5 Magnetic field (H) dependent magnetization (M) of $Bi_{3.9}Fe_{0.1}O_4S_3$ sample at several different temperatures in an applied field up to 5 k Oe. **a** Isothermal magnetization with field (M–H) at 2, 3 and 4 K in an applied field up to 5 k Oe. **b** Isothermal magnetization with field (M–H) at 10 K in an applied field up to 4 k Oe. **c** The enlarged view of isothermal magnetization with field (M–H) at 4 K in an applied field up to 4 k Oe

in $Bi_{4-x}A_xO_4S_3$ (A = Fe, Mn, Co and Ni) via the *RKKY* interaction.

To reveal the ferrimagnetic behaviors in $Bi_{4-x}Fe_xO_4S_3$ samples, we measure magnetic field (H) dependence of magnetization (M) for $Bi_{3.9}Fe_{0.1}O_4S_3$ ceramic at several different temperatures. Figure 5a shows the isothermal magnetization curve (M–H) at 2, 3 and 4 K with an applied field up to 5 k Oe and we can clearly see the superconductivity features associated with each M–H loop. Reasonably, these features diminish with the increase of temperature. In contrast, the behavior in high temperature is manifested in Fig. 5b. The M–H loop at $T = 10$ K reveals a standard magnetic hysteresis loop for a

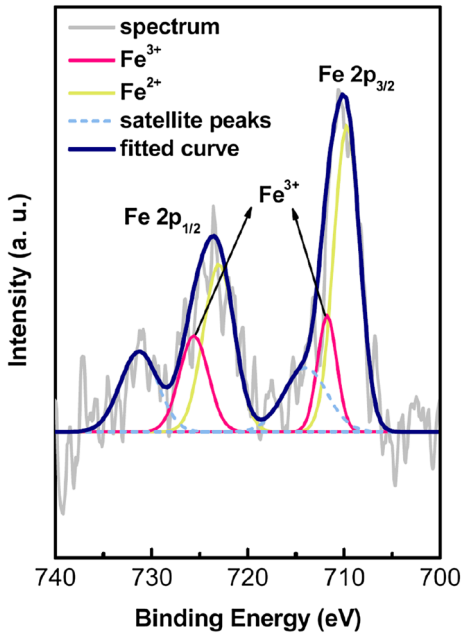

Fig. 6 X-ray photoelectron spectroscopy of sample $Bi_{3.9}Fe_{0.1}O_4S_3$. Analysis of the XPS data of $Bi_{3.9}Fe_{0.1}O_4S_3$, showing the valences of Fe ions being Fe^{2+} (primary) and Fe^{3+} (secondary)

ferromagnetic material. Same as the M–H loops for $Bi_{3.9}Co_{0.1}O_4S_3$ ceramic [24], $Bi_{3.9}Fe_{0.1}O_4S_3$ sample also appear as superconducting currents at $T < T_C$, as shown in Fig. 5c. The enlarged view of M–H loop (Fig. 5c) of $Bi_{3.9}Fe_{0.1}O_4S_3$ ceramic could be separated into weak ferromagnetic and superconducting loops. Therefore, the weak ferromagnetic behavior in M–H loops may come due to the different magnetic moment of Fe^{2+} and Fe^{3+}ions. It can be confirmed from our XPS studies.

The results for both enhanced superconductivity and long-range ferrimagnetism in the $Bi_{4-x}Fe_xO_4S_3$ ($0 \le x \le 0.1$) ceramics may be understood by investigating the valences of the Fe ions in the $Bi_{3.9}Fe_{0.1}O_4S_3$ compound. The XPS measurements show that the valence of Fe ions is primarily +2 and then +3, as shown in Fig. 6. The substitution of Fe^{2+} and Fe^{3+} for Bi^{3+} provides equal carriers for BiS_2 conducting layers. So T_C from resistivity data is not suppressed by increasing the Fe doping level. On the other hand, the magnetic moments of dilute Fe ions are primarily confined and coupled via the *RKKY* interaction [28] within the block layers. Therefore, the resulting ferrimagnetism does not directly influence the cooper pairing within the BiS_2 layers.

4 Summary

Polycrystalline $Bi_{4-x}Fe_xO_4S_3$ ($0 \le x \le 0.1$) samples were synthesized and their physical properties are studied. The magnetization susceptibility results reveal the coexistence

of long-range ferrimagnetism and superconductivity for the first time in $Bi_{4-x}Fe_xO_4S_3$ ($0 \leq x \leq 0.1$) system. The isothermal magnetization curves (M–H) show a weak ferromagnetism due to the different magnetic moment of Fe^{2+} and Fe^{3+} ions. Furthermore, the resistivity and magnetization susceptibility results imply the superconducting transition temperature that increased gradually to the maximum when $x = 0.05$ and then suppressed with further doping. The enhancement of T_C in lower doping level in $Bi_{4-x}A_xO_4S_3$ (A = Fe and Mn, Co, Ni) may indicate that the $Bi_4O_4S_3$ crystal and band structure can be optimized by doping magnetic transition mental ions such as Fe, Mn, Co and Ni. However, the microscopic interplay between magnetism and superconductivity in the $Bi_4O_4S_3$ still need growth in single crystalline materials.

Acknowledgements Financial support to this work from the National Key Research and Development Program of China (2016YFB0700504) is gratefully acknowledged. We acknowledge the following funding: Shanghai Pujiang Program (13PJD015), Science and Technology commission of Shanghai Municipality (13ZR1415200, 13JC1402400), and National Natural Science Foundation of China (51372149, 51371111). The authors thank beamline BL14B1 of Shanghai Synchrotron Radiation Facility. We thank Zhe Li and Jingzhe Chen for their help on the english improvement and lattice constants calculation.

References

1. J.G. Bednorz, K.A. Muller, Z. Für Phys. B Condens. Matter **64**, 189 (1986)
2. Y. Kamihara, T. Watanabe, M. Hirano, H. Hosono, J. Am. Chem. Soc. **130**, 3296 (2008)
3. X.H. Chen, T. Wu, G. Wu, R.H. Liu, H. Chen, D.F. Fang, Nature **453**, 761 (2008)
4. Y. Mizuguchi, H. Fujihisa, Y. Gotoh, K. Suzuki, H. Usui, K. Kuroki, S. Demura, Y. Takano, H. Izawa, O. Miura, Phys. Rev. B **86**, 220510 (2012)
5. C. Morice, E. Artacho, S.E. Dutton, D. Molnar, H.-J. Kim, S.S. Saxena, J. Phys. Condens. Matter Inst. Phys. J. **27**, 135501 (2015)
6. H. Takatsu, Y. Mizuguchi, H. Izawa, O. Miura, H. Kadowaki, J. Phys. Soc. Jpn. **81**, 125002 (2012)
7. S.K. Singh, A. Kumar, B.G. Shruti, G. Sharma, S. Patnaik, V.P.S. Awana, J. Am. Chem. Soc. **134**, 16504 (2012)
8. V.P.S. Awana, A. Kumar, R. Jha, S. Kumar Singh, A. Pal, J.Saha Shruti, S. Patnaik, Solid State Commun. **157**, 21 (2013)
9. S. Demura, Y. Mizuguchi, K. Deguchi, H. Okazaki, H. Hara, T. Watanabe, S.J. Denholme, M. Fujioka, T. Ozaki, H. Fujihisa, Y. Gotoh, O. Miura, T. Yamaguchi, H. Takeya, Y. Takano, J. Phys. Soc. Jpn. **82**, 033708 (2013)
10. Y. Mizuguchi, T. Hiroi, J. Kajitani, H. Takatsu, H. Kadowaki, O. Miura, J. Phys. Soc. Jpn. **83**, 053704 (2014)
11. R. Jha, H. Kishan, V.P.S. Awana, J. Appl. Phys. **115**, 013902 (2014)
12. J. Xing, S. Li, X. Ding, H. Yang, H.-H. Wen, Phys. Rev. B **86**, 214518 (2012)
13. R. Jha, A. Kumar, S. Kumar, Singh, and V. P. S. Awana. J. Supercond. Nov. Magn. **26**, 499 (2013)
14. X. Lin, X. Ni, B. Chen, X. Xu, X. Yang, J. Dai, Y. Li, X. Yang, Y. Luo, Q. Tao, G. Cao, Z. Xu, Phys. Rev. B **87**, 8691 (2013)
15. R. Jha, B. Tiwari, V.P.S. Awana, J. Phys. Soc. Jpn. **83**, 063707 (2014)
16. R.J. Cava, B. Batlogg, J.J. Krajewski, R. Farrow, L.W. Rupp, A.E. White, K. Short, W.F. Peck, T. Kometani, Nature **332**, 814 (1988)
17. P.A. Lee, N. Nagaosa, X.-G. Wen, Rev. Mod. Phys. **78**, 17 (2006)
18. R. Zhou, Z. Li, J. Yang, D.L. Sun, C.T. Lin, G. Zheng, Nat. Commun. **4**, 2265 (2013)
19. T. Oka, Z. Li, S. Kawasaki, G.F. Chen, N.L. Wang, G. Zheng, Phys. Rev. Lett. **108**, 047001 (2012)
20. M. Hirano, Y. Yamada, T. Saito, R. Nagashima, T. Konishi, T. Toriyama, Y. Ohta, H. Fukazawa, Y. Kohori, Y. Furukawa, K. Kihou, C.-H. Lee, A. Iyo, H. Eisaki, J. Phys. Soc. Jpn. **81**, 054704 (2012)
21. S. Demura, K. Deguchi, Y. Mizuguchi, K. Sato, R. Honjyo, A. Yamashita, T. Yamaki, H. Hara, T. Watanabe, S.J. Denholme, M. Fujioka, H. Okazaki, T. Ozaki, O. Miura, T. Yamaguchi, H. Takeya, Y. Takano, J. Phys. Soc. Jpn. **84**, 024709 (2015)
22. L. Li, Y. Li, Y. Jin, H. Huang, B. Chen, X. Xu, J. Dai, L. Zhang, X. Yang, H. Zhai, G. Cao, Z. Xu, Phys. Rev. B **91**, 4508 (2015)
23. X. Yin, Z. Feng, C. Yu, Q. Li, Y. Cao, B. Kang, B. Lu, J. Chen, T. Gao, X. Li, J. Guo, H. Chu, G. Wang, D. Deng, C. Jing, S. Cao, J. Zhang, J. Supercond. Nov. Magn. **29**, 879 (2016)
24. C. Yu, Z. Feng, X. Yin, Q. Li, B. Kang, B. Lu, C. Jing, S. Cao, J. Zhang, Phys. C Supercond. **528**, 23 (2016)
25. Z. Feng, X. Yin, Y. Cao, X. Peng, T. Gao, C. Yu, J. Chen, B. Kang, B. Lu, J. Guo, Q. Li, W.-S. Tseng, Z. Ma, C. Jing, S. Cao, J. Zhang, N.-C. Yeh, Phys. Rev. B **94**, 064522 (2016)
26. V.N. Nikiforov, Y.A. Koksharov, S.N. Polyakov, A.P. Malakho, A.V. Volkov, M.A. Moskvina, G.B. Khomutov, V.Y. Irkhin, J. Alloys Compd. **569**, 58 (2013)
27. N. Andrei, K. Furuya, J.H. Lowenstein, Rev. Mod. Phys. **55**, 331 (1983)
28. M.A. Ruderman, C. Kittel, Phys. Rev. **96**, 99 (1954)